Identifying the mechanisms of concrete drying: An experimental-numerical approach

Jérôme Carette, François Soleilhet, Farid Benboudjema, Xiaoyan Ma, Georges Nahas, Kamilia Abahri, Aveline Darquennes, Rachid Bennacer

Identifying the mechanisms of concrete drying: an experimental-numerical approach

Jérôme Carette[(1,2,3)], François Soleilhet[(1)], Farid Benboudjema[(1)], Xiaoyan Ma[(1)], Georges Nahas[(1,2)], Kamilia Abahri[(1)], Aveline Darquennes[(4)], Rachid Bennacer[(1)]

[(1)] LMT, ENS Cachan, CNRS, Université Paris-Saclay, 94235 Cachan, France

[(2)] IRSN, Fontenay-aux-Roses, FRANCE

[(3)] Université libre de Bruxelles (ULB), Avenue Franklin Roosevelt 50, 1050 Bruxelles, Belgium

[(4)] Institut National des Sciences Appliquées de Rennes, Rennes, France

Abstract

The loss of non-chemically linked water from concrete has a significant effect on its structural behaviour through a modification of its strength, Young modulus, fracture properties, creep and volume stability. The knowledge of the hydric state of concrete is therefore of upmost importance regarding the mechanical behaviour and durability potential of concrete structures. We use a non-linear diffusion equation for predicting the drying kinetics, including processes of the diffusion of water vapour and the permeation of liquid water. The multiple parameters of this model are then identified based on an in-house optimization algorithm and on a thorough experimental setup including measurements of mass loss and located relative humidity evolutions on various sample geometries. This coupled experimental and numerical approach allows identifying robust and meaningful material parameters of concrete used for drying predictions. This approach allows also identifying the mechanisms in concrete drying phenomena and processes by inverse analysis

Keywords : Concrete drying, relative humidity, transport properties

1. Introduction

Concrete subjected to drying quickly develops strong inner gradients of water content. The loss of non-chemically linked (or free) water from a concrete has a significant effect on its structural behaviour through a modification of its strength [POP86], Young modulus [BAO14], fracture properties and creep [BAZ94]. The water loss also induces drying shrinkage [KIM98] and drying creep [GAM78], which induce deformation of higher magnitude than the autogenous deformation [ZHA11]. This contributes to deflection and cracking (due to drying gradients with shrinkage induced cracking, but also strains incompatibilities between cement paste and aggregates [BIS02]). It also may induce prestress loss. In addition, the concrete diffusivity and

permeability are highly affected by its water content [MIL61, MUA76, VAN80, HUA15, ZHA16], thus affecting its durability potential. The knowledge of the hydric state of concrete is therefore of upmost importance regarding the mechanical behaviour and durability potential of concrete structures.

The widest used measurement to characterize the hydric state of the concrete is the weight loss in drying conditions. However, this macroscopic measurement does not allow obtaining the distribution of the degree of saturation inside the specimen. Transport properties (porosity, liquid and gas permeability, diffusivity) can also be measured, but they generally suffer from hypothesis and shortcomings (cracking for instance if the material is completely dried to determine intrinsic gas permeability) that prevent these values to be used as is in a complete multi-parameter drying model. Moreover, measurements of water permeability by imposing a gradient of pressure in saturated conditions are very sensitive to the preparation of the samples (pre-dried specimens show greated "intrinsic permeability" due to drying cracks, [HAL00]). Rather, they are very powerful in order to compare different concrete compositions. This is why indirect methods are generally used to determine the moisture (or degree of saturation) gradient present in the material. These methods include electromagnetic methods [SBA07], ultrasonic methods [POP05, SBA12], X-ray tomography [JER15], or relative humidity measurement [GRA14, ZHA15, HUA15]. All these possibilities are based on physical indicators that are dependent on the water content. In order to get the actual saturation degree of the material from these measurements, calibration curves are necessary. This calibration is specific to each method, and the protocol required for its determination is not straightforward. In the case of the measurement of relative humidity, obtaining the degree of saturation relies on the knowledge of desorption isotherms of the material. Even if the measurement of relative humidity (RH) is generally local and does not allow a full mapping of the water content of concrete, the advantage of this method is that concrete desorption isotherm has been widely studied in the last decades [XI94, BAR07, ZHA14, ZHA16]. Therefore, the determination of the saturation degree from local RH measurements is straightforward during desaturation of the material.

In any case, the experimental determination of the hydric state of concrete during drying is complex, thus justifying the many modelling approaches for the water transport in unsaturated porous media, and in particular in concrete [KIM98, MUA76, VAN80, HUA15, ZHA15, ZHA14].

In this paper, the drying of various concrete samples is cautiously studied through refined measurement of the mass loss (global measurement) and internal relative humidity distribution (local measurement). Various sample sizes and shapes are tested. From the results of these tests, the values of the model input parameters are assessed through the use of an in-house identification tool. The variation of these parameters as well as the relevance of performing combined measurements of the global and local measurements of the hydric state of concrete is discussed.

2. Drying model

In order to be accurate, our model includes predictive transfer equations as well as the non-linear coefficients that control the transfer, completed by realisticapplied boundary conditions.

2.1. *General expression*

In the concrete porosity, two main phases coexist. The solid phase and the liquid phase (liquid water and vapour water). The amount of each phase depends on parameters such as porosity, tortuosity, connectivity, ambient conditions and material saturation. These phases are not pure (presence of chloride ions for instance). Within the material, different exchanges are set up in the form of mechanisms such as permeation of liquid water as well as diffusion of the water vapour.
The drying model used in this study is based on the one developed by [MAI01]. It can be written in the form of a non-linear diffusion equation (equation **Erreur ! Source du renvoi introuvable.**) [BAR07b]. The apparent coefficient of water diffusion D_w is a function of the degree of saturation S, and is considered to combine two main mechanisms, which are the diffusion of water vapour and the permeation of liquid water. The water diffusion coefficient is computed according to equation **Erreur ! Source du renvoi introuvable.**, where K_l and D_v are non-linear coefficient relative to the transport of liquid water and water vapour respectively. While it is known that permeation is clearly predominant for high saturation and that diffusion is predominant for low saturation, there is currently no clear consensus as to which is the predominant mechanism in intermediate saturation degrees, especially when hydraulic gradients are considered

$$\frac{\partial S}{\partial t} = div\left(D_w \overrightarrow{grad}(S)\right) \tag{1}$$

$$D_w = K_l + D_v \tag{2}$$

All these exchanges are considered as isotherm (latent heat of vaporization of water is not taking into account). The material is assumed to be mature and dimensionally stable (no interaction between drying and drying shrinkage). The contribution of dry air to the mass transport is neglected [ZHA16]. If the concrete porous network is saturated, the permeation mechanism is the predominant one, whereas for a low degree of saturation, the movement of water in the form of vapour diffusion cannot be neglected.
The liquid water flow can be expressed through Darcy's law, which relates the fluid mass flow through a medium to the pressure gradient of this fluid, as expressed in equation (3). In which k_{la} is the concrete apparent permeability to liquid water(m^2), μ_l is the dynamic viscosity of water $(Pa \cdot s)$, ρ_l is the water density$(kg \cdot m^{-3})$, P_l is the liquid water pressure (Pa), and J_l is the liquid water flux$(kg \cdot m^{-2} \cdot s^{-1})$.

$$\overrightarrow{J_l} = -\rho_l \frac{k_{la}}{\mu_l} \overrightarrow{grad}(P_l) \tag{3}$$

The water vapour flow can be expressed with Fick's law, representing the flow of water in form of vapour due to a gradient in relative humidity in concrete. It can be expressed in the form of equation (4), where J_v is the water vapour flux $(kg \cdot m^{-2} \cdot s^{-1})$, D_{va} is the apparent diffusion coefficient of water vapour in air $(m^2 \cdot s^{-1})$, P_v is the partial vapour pressure (Pa), M_w is the molecular mass of water $(kg \cdot mol^{-1})$, R is the gas constant $(J \cdot K^{-1} \cdot mol^{-1})$ and T is the temperature (K).

$$\overrightarrow{J_v} = -D_{va} \frac{M_w}{RT} \overrightarrow{grad}(P_v) \tag{4}$$

As shown in equation (5), the difference between the gas pressure P_g (Pa) and liquid water pressure is the capillary pressure P_c (Pa). According to Kelvin's equation, the relationship between the capillary forces and the relative humidity in concrete can be expressed as shown in equation (6), where h is the relative humidity, since P_g is considered constant and equal to atmospheric pressure.

$$P_c = P_g - P_l \tag{5}$$

$$P_c = \frac{-\rho_l R T ln(h)}{M_w} \tag{6}$$

2.2. Non-saturated concrete behaviour

In this model, the main unknown is chosen to be the relative humidity. This is why all further equations are expressed as function of that parameter. The desorption isotherm links the saturation degree to the relative humidity. The most common equation used to model this relationship is the van Genuchten equation [VAN80] (equation **Erreur ! Source du renvoi introuvable.**), where a_{vg}, b_{vg} and c_{vg} are three parameters that can be obtained from experimental results of the desorption isotherm for the tested material. A commonly used restriction is applied on the value of c_{vg}, as shown in equation **Erreur ! Source du renvoi introuvable.**.

$$S = \left(1 + \left(-a_{vg} ln(h)\right)^{b_{vg}}\right)^{-c_{vg}} \tag{7}$$

$$\mathrm{c}_{vg} = 1 - \frac{1}{b_{vg}} \tag{8}$$

From combining equations (3) to (6) with mass balance principles, the equation that has to be solved for the moisture transport can be expressed as equation **Erreur ! Source du renvoi introuvable.**, where Φ is the concrete water porosity and P_v^{sat} is the saturation vapor pressure (Pa).

$$\Phi \frac{\partial S}{\partial h}\frac{\partial h}{\partial t} = \frac{1}{\rho_l} div\left(\vec{J_l} + \vec{J_v}\right) = div\left[\left(-\frac{k_{la}\,\rho_l\,R\,T}{\mu_l\,M_w\,h} - \frac{D_{va}\,M_w\,P_v^{sat}}{\rho_l\,R\,T}\right)\overrightarrow{grad}(\mathrm{h})\right] \tag{9}$$

The dependency of k_{la} to the degree of saturation can be taken into account with equation (10), where k_l (m²)is the intrinsic water permeability of concrete in saturated conditions, and k_{rl} is the relative permeability. The relative permeability can be determined through the Mualem conceptual relationship [MUA76] shown in equation (11), where a_{mu} and b_{mu} are material parameters. Generally, the parameter a_{mu} is considered equal to parameter c_{vg}. While the used model considers these parameters equal, it leaves the opportunity to uncouple them during their identification process.. For cement-based materials, the recommended value for b_{mu} is within the large range of -4 to 5.5 [MON04, LEE08, POY11, ZHO14].

$$k_{la}(S) = k_{rl}\,k_l \tag{10}$$

$$k_{rl}(S) = S^{b_{mu}}\left(1 - \left(1 - S^{\frac{1}{a_{mu}}}\right)^{a_{mu}}\right)^2 \tag{11}$$

$$D_{va}(S) = d_{rl}\, D_0 \tag{12}$$

$$d_{rl}(S) = \Phi^{a_{mq}}\,(1-S)^{b_{mq}} \tag{13}$$

In the same way, the diffusion of water vapour is highly dependent on the saturation degree. The tortuosity of the concrete porosity also affects this parameter. The empirical model shown in equation (13) and (13) was developed in order to take both parameters into account [MIL61]. The apparent diffusion is related to the relative diffusion function d_{rl} and to the diffusion coefficient of water vapour in air D_0. The parameters a_{mq} and b_{mq} can yield variable values between 1.3 and 2.74 for one and 3.3 and 4.2 for the other, respectively [THI07]. However, since these parameters are relative to the tortuosity of the material, it is to be expected that their value is depending on the concrete pore structure.

Based on the above equations, the respective contributions of liquid water permeability and water vapor diffusion to the apparent water diffusion coefficient can be expressed with equations (14) and (15).

$$K_l(S) = -\frac{k_{la}\,\rho_l\,R\,T}{\mu_l\,M_w\,HR\,\Phi}\frac{dh}{dS} \tag{14}$$

$$D_v(S) = -\frac{D_{va}\,M_w\,P_v^{sat}}{\rho_l\,R\,T\;\;\Phi}\frac{dh}{dS} \tag{15}$$

2.3. ***Boundary conditions***

Various types of boundary conditions are generally considered for modelling concrete drying. First, it is possible to impose the outdoor relative humidity directly at the air-concrete interface [HIL14, OXF16]. However, this does not take into account the presence of a so-called boundary layer of air at the air-concrete interface whose moisture content depends on the distance to the concrete surface. The thickness of this boundary layer strongly depends on the ambient conditions (wind speed, temperature) and the material surface condition (surface porosity, surface roughness, and surface moisture) [ZHA15]. Generally, this boundary condition can be taken into account in the form of equation (16), where δ is the size of the boundary layer (in m), or more generally by equation (17) [SAK83, HUA15, ZHA15, OZB16]. The area factor h_{CL} reaches values varying by several orders of magnitude depending on the study. A study suggests the value of 1.5×10^{-5} [HUA15]. According to [OZB16, AKI97], its value ranges from 8×10^{-7} to 2×10^{-6} for w/c ranging from 0.43 to 0.55 respectively. According to other authors, it can reach much higher values in the range of 10^{-3} to 10^{-2} [SAK83, ZHA15].

$$J_{CL} = -D_0\,\frac{M_w P_{vs}}{RT}\;\;\frac{h_s - h_e}{\delta} \tag{16}$$

$$J_{CL} = -\,h_{CL}.(h_s - h_e) \tag{17}$$

3. Materials and methods

The tested concrete composition is referred to as B11 concrete. Three sample geometries for different drying patterns are placed in a storage bin and mass loss and relative humidity are

recorded regularly. With the experimental data obtained in this study, a finite element simulation is performed and an identification procedure is developed on Matlab to find out the optimised parameters.

*3.1.**Concrete composition***

The composition of B11 concrete and major properties are shown in Table 1. It has been widely studied in previous studies [BRI11, HIL14] and its mechanical properties are therefore mostly known, including its density and water porosity. The mixing procedure is as follows : the dry materials (aggregates, sand and cement) are mixed for 60 seconds. Then, water and 1/3 of the superplasticizer are added with further mixing during 150 seconds. Then, the rest of the superplasticizer is included, followed by 90 additional seconds of mixing. 30L of concrete were mixed in one batch.

Table 1. B11 mix design and main properties [HIL14]

	B11 [kg/m³]	***w/c***	[-]	0.573
Cement (CEM II Airvault Calcia)	336	ρ	[kg/m^3]	2324
Sand (0/4)	740	**Slump**	[cm]	8-11
Aggregates (4/12.5)	303	**Porosity**	[-]	13.2-13.8
Aggregates (10/20)	752	f_c (28 days)	[MPa]	46.5
Water	193	f_t (28 days)	[MPa]	3.29
Superplasticizer (Plastiment HP)	1.174	***E*** (28 days)	[GPa]	31.34

*3.2.**Test setup***

In order to ensure the same controlled curing conditions to all concrete specimens (temperature T and relative humidity RH), a large storage bin is developed. The use of a climatic chamber is rejected due to the difficulty of limiting the forced convection on the faces subjected to drying, and of ensuring the uniformity of this phenomenon on all sides and on all samples. The storage bin is impermeable to air and moisture.

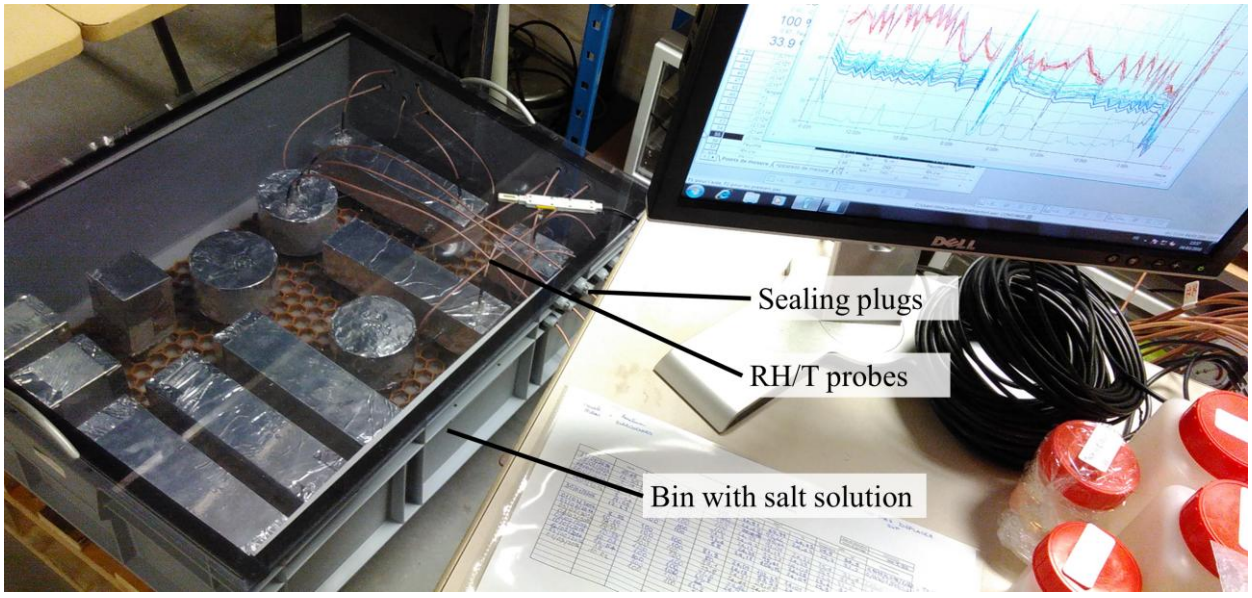

Figure 1. Experimental setup linked to the continuous measurement of RH and T sensors

In order to enable placing several temperature and relative humidity sensors inside the storage bin, holes are performed, and sealing plugs are installed. The concrete samples are placed on a plastic honeycomb duckboard allowing maximized interaction between the salt solution and the ambient air. This setup is shown in Figure 1. The saturated salt solution is prepared using potassium carbonate in order to reach an ambient RH of 45%. The room temperature is controlled at 25 ± 1°C (this has been checked using the probes).

The concrete samples are prevented from drying until the test starts, which occurred two months after mixing. Due to the high w/c ratio of the B11 concrete, weconsider that the hydration reactions are almost completed and that the auto-desiccation phenomenon can be neglected [BRI11]. The initial state of the material is therefore not fully saturated, but with a very high saturation degree due to the high w/c ratio of the B11 concrete.

The experimental measurements consist in mass loss measurements at regular intervals and of the internal relative humidity in concrete samples at various distances from the drying interface. Three sample geometries are considered (see Figure 2):

- G1: 70x70x280mm prism, drying on the two opposite lateral faces (5 samples),
- G2: 70x70x110mm prism, drying on the two opposite lateral faces (3 samples),
- G3: 70x110mm cylinder, drying in the radial direction (3 samples),

For each of these geometries, the average drying radius (r_d, in m) is computed as the ratio between the drying surface and the sample volume. This results in r_d of 0.14, 0.055 and 0.0275 and for geometries G1, G2 and G3 respectively.

The mass loss measurements are performed on 3 samples for G1 and on 2 samples for G2 and G3. This study focuses on the first few weeks after drying is initiated. The relative humidity is measured at various distances from the drying interface on geometries G1, G2 and G3 according to the distribution shown in Figure 2. The used sensors are capacitive probes Ahlborn FHA 646 R. These probes are chosen due to their extremely small dimensions (5 mm diameter) as well as their high accuracy and wide operating RH and T range. The RH sensors are placed inside concrete through holes drilled on hardened concrete. This method is considered more appropriate than reservations in concrete from the casting since the latter results in a layer of mortar around the hole that is not representative of the tested material. In order to avoid damaging the sample, 6 mm diameter holes are obtained by drilling with progressively increased diameter from 3 mm to 6 mm.

All sensors are placed in 30mm deep reservations obtained by perforation of the hardened concrete. Sensors are placed in the centre of each sample. In geometry G1, additional sensors are placed at 15, 30, and 60 mm from each drying interface. In geometries G2 and G3, two additional sensors are placed at 15 mm from the drying interface.

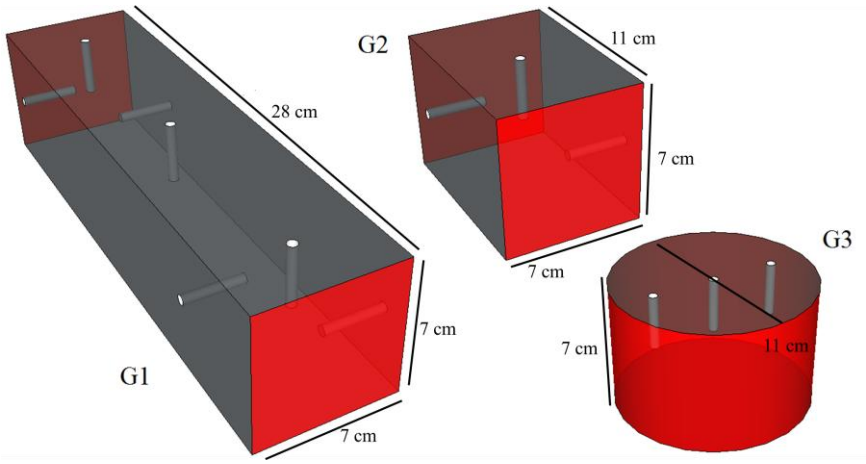

Figure 2. Layout plan of RH sensors (sides submitted to drying displayed in red : two opposite lateral faces for G1 and G2, drying in the radial direction for G3)

3.3. *Identification procedure*

In this study, an identification procedure based on Finite Element Modelling Updating (FEMU) [NEG15] was developed using Cast3m [CAS07] and Matlab. This method (FEMU) is based on the minimisation of an error function built with the difference between data gathered from experimental work and numerical results. The identification flow chart is presented in Figure 3. It can be divided into three parts. The first is related to the experimental data obtained in this study. Then, a second part is related to the FE simulation. The last part is associated with the minimization algorithm, developed on Matlab.

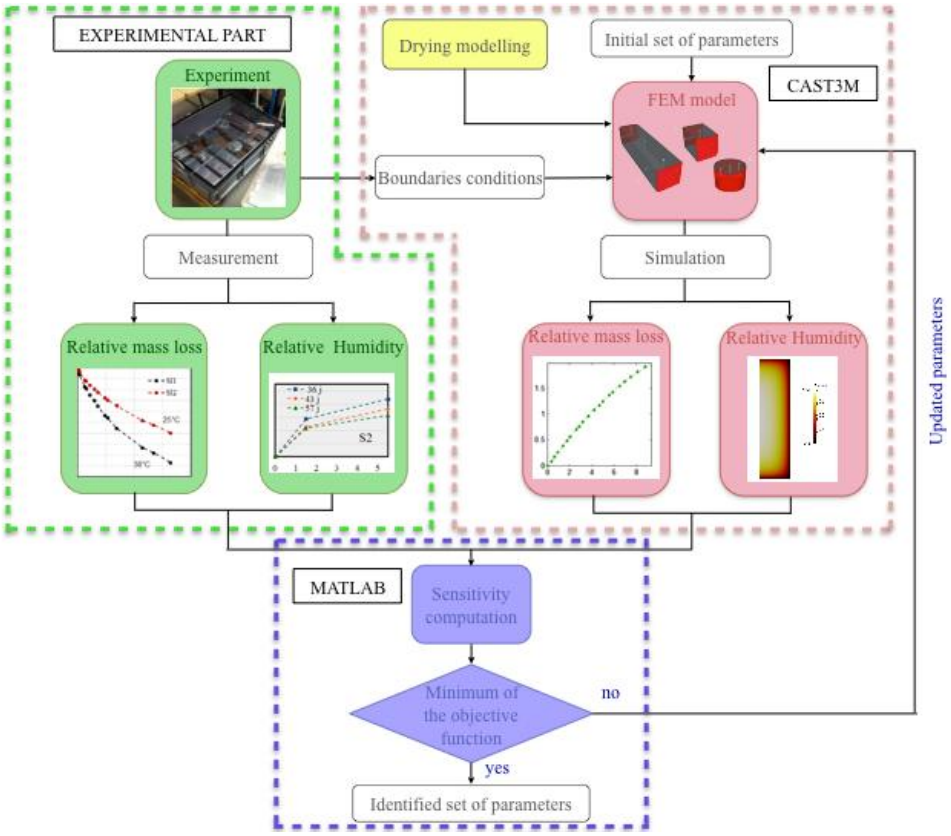

Figure 3. Identification algorithm flow chart

This inverse modelling relies on a priori knowledge of the drying model and its ability to accurately predict the drying process. In this case, the used numerical model was presented in section 2. Thus, the experimental process is simulated with relative humidity and temperature as boundary conditions of the modelling. It is then possible to build an error function, shown in Eq. (18). This error function $\vec{f}$ includes experimental data (indicated by the *e* exponent), simulated data (indicated by the *s* exponent), as well as results from mass loss measurements (indicated by the *ML* index) and from relative humidity measurements (indicated by the *RH* index). This function ensures that:

- More relative importance is assigned to higher mass loss or lower relative humidity,
- The same relative importance is assigned to mass loss resulting from one sample and to relative humidity measurements resulting from one sensor,
- Several samples or sensors for the same measurement can easily be included independently from one another in the identification process.

$$\vec{f} = \sum_{samples} \left[\frac{\vec{C}^{e}_{ML}}{max(\vec{C}^{e}_{ML})} - \frac{\vec{C}^{s}_{ML}(\vec{p})}{max(\vec{C}^{s}_{ML})} \right] + \sum_{sensors} \left[\frac{\vec{C}^{e}_{HR}}{max(100 - \vec{C}^{e}_{HR})} - \frac{\vec{C}^{s}_{HR}(\vec{p})}{max(100 - \vec{C}^{s}_{HR})} \right] \quad (18)$$

where C^e and C^s are the vectors of experimental and modelling results for respectively the relative mass variation (ML) and the relative humidity values (RH). $\vec{p}$ is a vector composed of model's input parameters. It is possible to add weighting factors in this error function.

Finally, the minimisation is calculated, based on Levenberg-Marquart's optimisation method implemented in Matlab. The framework of the algorithm is presented in Figure 4.

Algorithm 1: Levenberg-Marquardt resolution

Input : Experimental points C_i^{exp}, $\boldsymbol{\delta}_{max}$;
Arbitrary initialization $\mathbf{p}_0$
begin
  k $\leftarrow 0$;
  $\theta \leftarrow 10^{-3}$;
  $\mathbf{J} \leftarrow \frac{dC}{d\mathbf{p}_0}$;
  $\mathbf{p} \leftarrow \mathbf{p}_0$;
  while *STOP-CRIT and* $(k < k_{max})$ **do**
    k $\leftarrow$ k+1 ;
    if $0 \equiv \sqrt{k} \pmod 2$ **then**
      Actualisation : $\mathbf{J} \leftarrow \frac{dC}{d\mathbf{p}_k}$;
    Get $C_i^{sim}(\mathbf{p})$ from simulation ;
    $\mathbf{f} \leftarrow C_i^{exp} - C_i^{sim}(\mathbf{p})$;
    $\lambda \leftarrow \theta\|\mathbf{f}\| + (1-\theta)\|\mathbf{J}^T\mathbf{f}\|$
    Find $\boldsymbol{\delta}$ such that $(\mathbf{J}^T\mathbf{J}\text{-}\lambda\ \mathbb{1})\ \boldsymbol{\delta} = \mathbf{J}^T\mathbf{f}$;
    if *abs* $(\boldsymbol{\delta}) \leq \boldsymbol{\delta}_{max}$ **then**
      $\mathbf{p} \leftarrow \mathbf{p} + \boldsymbol{\delta}$
    else
      $\mathbf{p} \leftarrow \mathbf{p} \pm \boldsymbol{\delta}_{max}$

Figure 4. Minimisation algorithm

The minimized parameters resulting from this process are entered in CAST3M as input parameters. The identification runs until it reaches a criterion based on the average relative increment of the identified parameters increments. If this average variation remains below the limit of 0.1% of the current parameters' values, the identification procedure is stopped.

Lastly, as our experimental work involves different shapes and dimensions, it is possible to diversify the identification process. Indeed, the process allows for identification of one or more shapes, and allows taking into account relative mass loss and relative humidity at the same time or separately.

4. Results

In this section, the measurement results of mass loss and relative humidity, as well as identification of model parameters is analysized.

4.1.Mass loss and relative humidity measurements

The mass loss (ML) due to water drying and the relative humidity (RH) evolution resulting from water transport are presented hereafter. First, it was verified that the RH sensors provide reproducible results, and that their presence does not affect the overall ML of drying samples. In order to do so, three G1 samples without drilled holes were tested in parallel with two G1 samples with drilled holes and RH sensors.

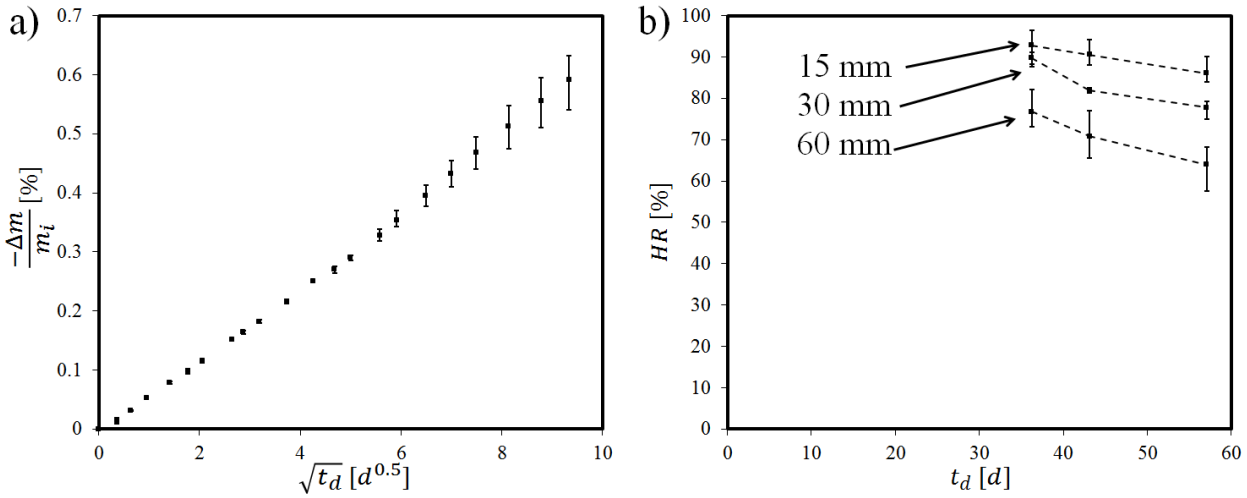

Figure 5. (a) Maximum, minimum and average values of relative mass loss for 5 G1 samples, with and without RH sensors (b) Maximum, minimum and average value of the RH measurement at three different distances from the drying interface from 3 G1 samples

The results shown in Figure 5(a) indicate that the variability on the ML measurement is low, and that the presence of the sensors do not affect the ML measurements. Mass loss being defined as a decrease of the mass through time, it is displayed as a positive value when drying occurs. On the other hand, the RH measurements are more variable, as displayed in Figure 5(b). This is most likely due to the heterogenous aspect of the concrete, for which the drilled holes (6 mm diameter, 30 mm depth) might be in contact with a variable amount of aggregate/mortar ratio. In addition, the presence of a large pore filled with water close to the drilled hole might locally affect the RH. Finally, local temperature gradients or discrepancies in the paricule size distribution can also

contribute to these variations. However, the general trend shown by all sensors is consistant, and the reproducibility of the measurement is satisfactory for the purpose of this study.

The mass loss observed in Figure 6(a) shows a very high dependency on the geometry. As the drying radius increases (meaning that the average distance between the free water and the drying interface increases), ML increases in a more slow and progressive way. Figure 6(b) represents ML as a function of the square root of time. In the first days after samples are submitted to drying, ML increases as a linear function of $t_d^{0.5}$, which is representative of processes that can be described by a diffusion-like differential equation.

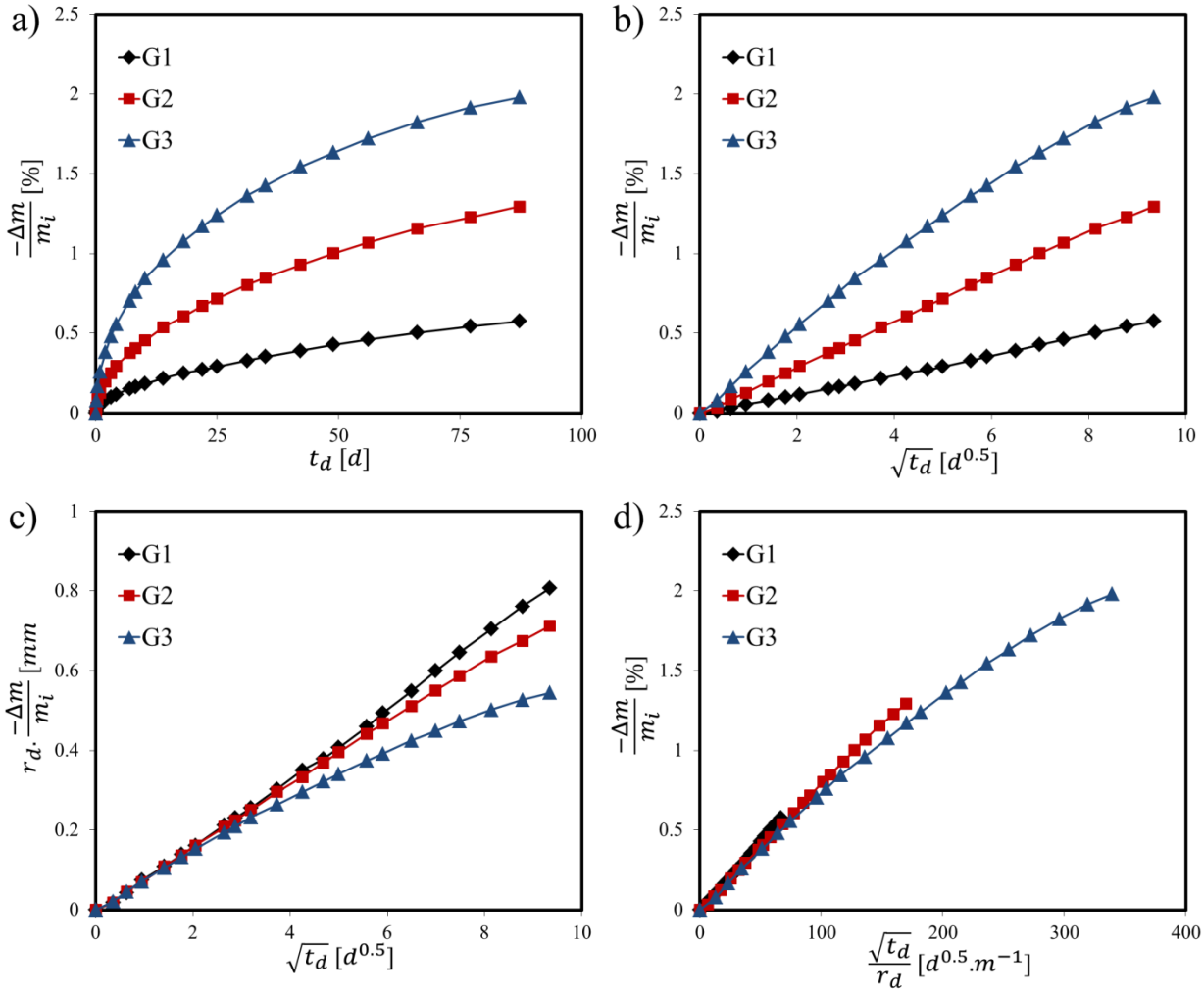

Figure 6. Mass loss of G1, G2 and G3 geometries expressed by (a) ML as a function of time (b) ML as a function of square root of time (c) ML multiplied by drying radius as a function of square root of time and (d) ML as a function of square root of time divided by drying radius

As drying occurs, the concrete saturation degree decreases. This leads to a variation of the transport properties of the material, and thus to the non-linear behaviour observed after a few weeks in G2, and after a few days in G3. This process is actually more visible in Figure 6(c), where ML is multiplied by the sample drying radius. This confirms that the initial slope of the ML-$t_d^{0.5}$ curve is independent on the geometry, and only depends on the material transport properties. This slope is therefore affected both by the concrete mix design and by its initial saturation degree. Then, as the drying radius decreases, the drying occurs faster, thus leading to a

decrease of the transport properties, and therefore to a decrease of the rate of ML. This observation can also be observed in Figure 6(d), in which ML is represented as a function of the square root of time divided by the drying radius. This figure actually shows that for a given mass loss, the rate of drying depends mostly on the time and drying radius. However, the G1, G2 and G3 curves are not superimposed, suggesting that the gradient of saturation degree inside the material also affects the drying behaviour. This observation highlights once again the importance of being able to measure and predict the water distribution inside the material in addition to global information such as mass loss measurements.

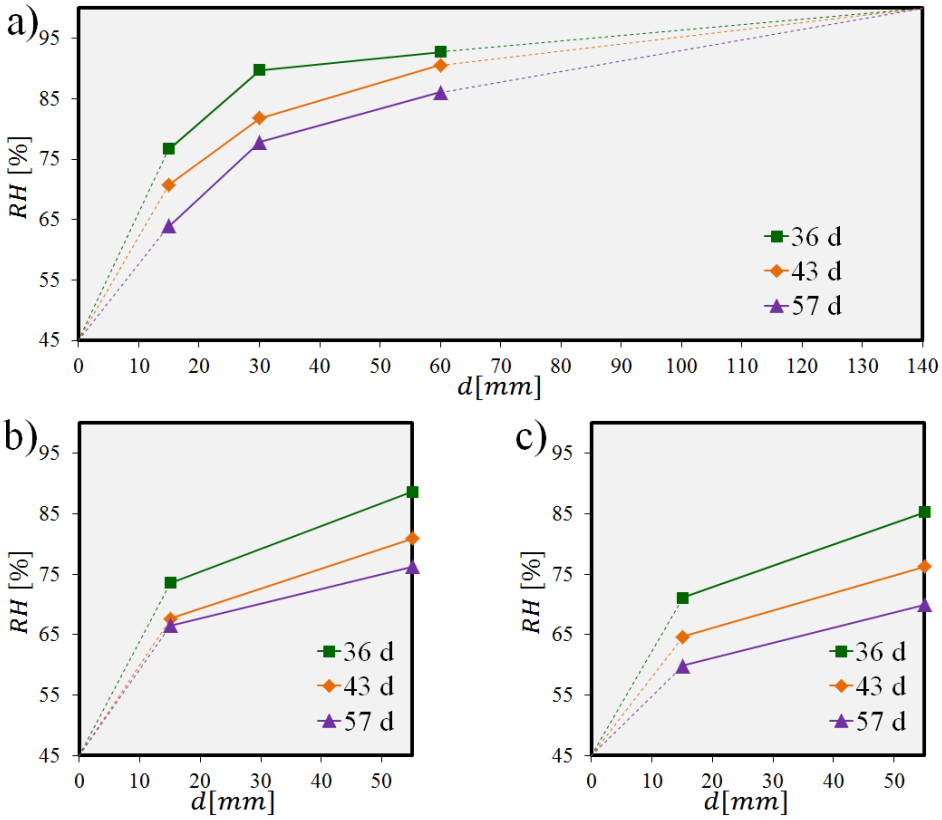

Figure 7. RH measurement inside the material at 36, 43 and 57 days as a function of the distance from the drying interface for geometry (a) G1 (b) G2 and (c) G3

Local RH measurements are performed in geometries G1, G2 and G3 at various distances from the interface. The results of these measurements are shown in Figure 7(a), (b) and (c) respectively. Only measurements when all sensors provide RH values under 95% are presented. This is due to the risk of condensation on the sensors for higher RH values, and to the limited accuracy of the sensors in such high RH environment. However, based on these measurements, it is considered that the RH in the centre of G1 is saturated through the whole experiment (3 months). This is represented by the dashed lines in Figure 7(a) between a distance of 60mm and 140 mm. In the same way, for representation purposes, it is considered in this section that the RH at the surface of the samples is equal to the RH of the ambient air, which is fixed at 45% through the whole test.

The results of Figure 7 show as expected that the RH profile decreases in proximity with the drying interface, due to the initially high humidity gradient between the concrete and the ambient air. Similarly, the RH profile decreases as the drying time increases. This phenomenon occurs in

every point of all geometries. Finally, as expected, at a given distance from the drying interface, at a given drying time, the local RH value is lower as the drying radius decreases. This is explained by the lower water supply of the core of the sample as the drying radius decreases, thus resulting in a lower RH for a similar amount of evaporated water. For instance, at 36 days, G2 shows an overall lower RH at 15 mm from the drying interface than G1. In the same way, G3 has a lower RH than G2 at 15 mm from the drying interface. The core RH of G3 is lower than the core RH of G2 even though both sensors are situated at the same distance to the surface due to the fact that G2 is a prismatic sample drying from the two opposite surfaces, whereas G3 is a cylinder drying from its whole circumference. This confirms the important effect of the drying radius.

*4.2.**Identification of model parameters***

The model described in section 2 is implemented in the CAST3M finite element software. The geometries are meshed with discretisation along the x-axis. More elements are placed in direct proximity with the drying interface due to the higher humidity gradient in that area. The meshing of G1 is given as an example in Figure 8, where only half of the prism is meshed since the test is symmetrical. The RH value is computed as the average value of the elements related to the position of the corresponding sensor S1, S3 or S3.

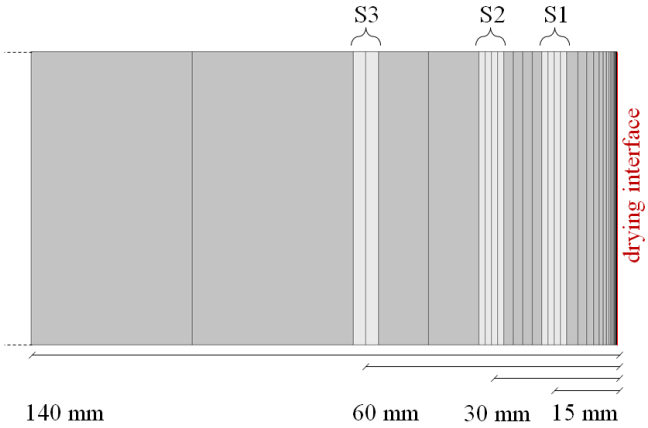

Figure 8. Meshing of G1 in the CAST3M software

In a first stage, inputs parameters for the model are extracted from the recommendations of the thesis A. Hilaire [HIL14], who worked on the same concrete. In addition, an exchange coefficient h_{CL} is chosen as equal to 10^{-5}. This value is extracted from previous research based on the coupled measurement and modelling of the surface RH of concrete during drying [CAR16]. Finally, the intrinsic permeability of concrete is manually modified in order to ensure a superimposition of the model mass loss in comparison with experimental values. A value of k_l of 1.13×10^{-21} m² is thus determined. This set of parameter (P1) is shown in Table 2, and results in the model-P1 curves in Figure 9(a) and (b).

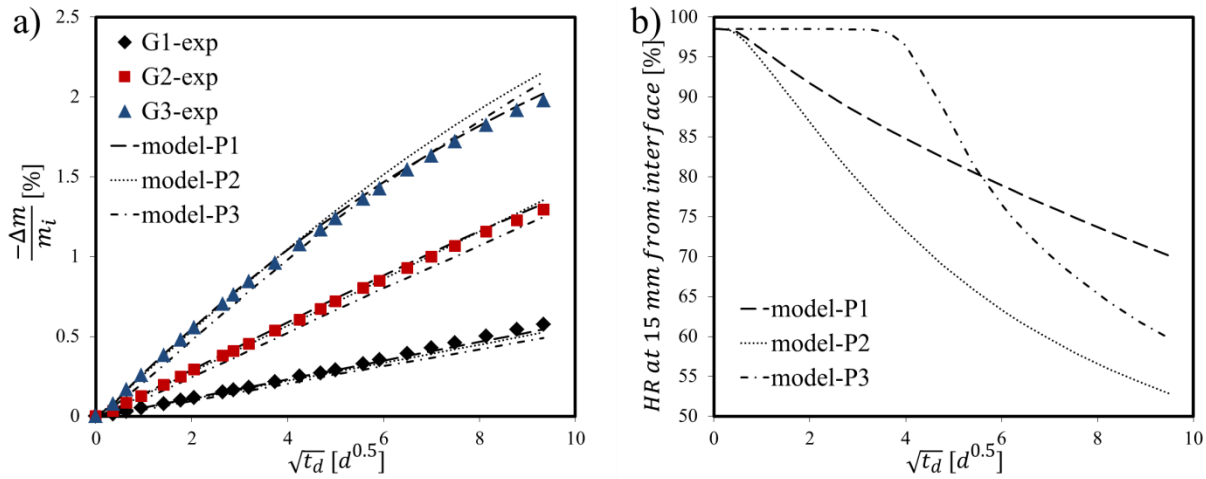

Figure 9. (a) experimental ML values and the corresponding simulation values for three sets of parameters P1, P2 and P3 (b) RH evolution at 15 mm from the drying interface in G3 resulting from sets of parameters P1, P2 and P3

Due to the large number of parameters in the drying model, several solutions can be found, all of them satisfying the mass loss curves of G1, G2 and G3. This is the case of sets of parameters P1, P2 and P3 (Table 2), all of which provide good superimposition of the experimental curves. However, the mass loss being a global measurement, it is shown in Figure 9(b) that these three sets of parameters do not provide the same hydraulic profiles inside the material. From a strictly modelling perspective, this is understandable, since a given saturation degree history (equivalent to the local distribution of the mass loss in the material) can result in variable relative humidity profile only by modifying the desorption isotherm values a_{vg}, b_{vg} or c_{vg}. This observation justifies the need to include additional experimental measurements in the parameter identification process. Indeed, based on the coupled measurement of the mass loss and RH at 15mm and 55mm from the drying interface, a new set of parameters can be determined (P4). This set of parameter provides an overall better representation of both measurements (Figure **10**10(a) and (b)).

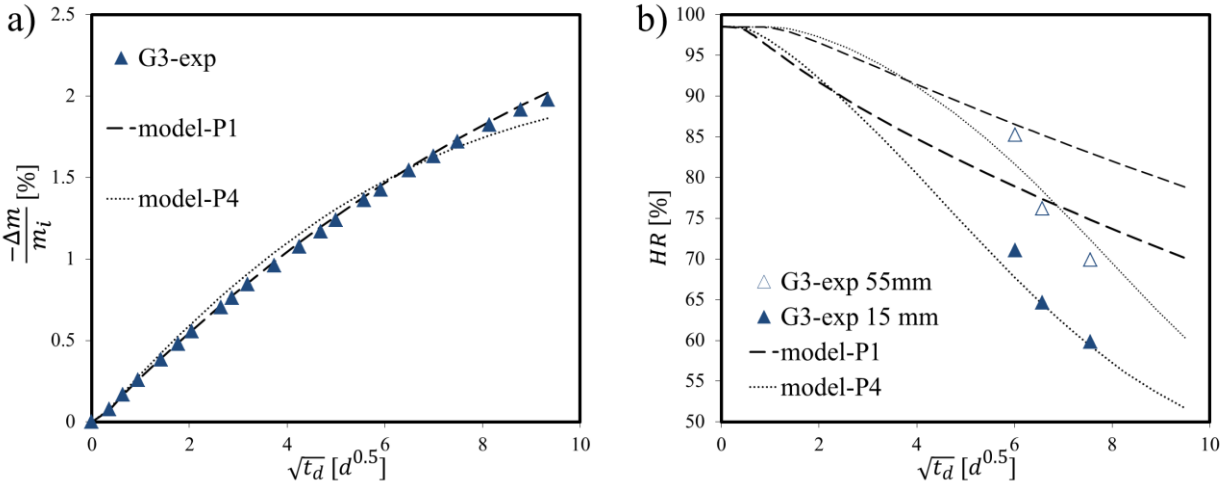

Figure 10. Experimental values and corresponding simulation of G3 for two sets of parameters P1 and P4 (a) mass loss and (b) relative humidity at 15 and 55mm from the drying interface

The developed identification algorithm is used in order to evaluate the effect of various experimental or simulation parameters on the identified parameters. The evaluated parameters

are the specimen geometry, the input parameters of the identification, the chosen model for the relative permeability function, and the temperature. This evaluation is made through comparison of the identified apparent coefficient of water diffusion D_w. For each case, this property is described as a function of the relative humidity, as well as its two contributing factors K_l and D_v.

4.2.1. *Effect of specimen geometry*

From a macroscopic phenomenological perspective, it is observed experimentally that the drying process is independent of the specimen geometry. For a given concrete, as the average drying radius decreases, the global mass loss decreases faster. The difference between G1, G2 and G3 observed in Figure 6 mostly come from the fact that a faster drying induces change in the transport properties due to the faster decrease of the water saturation. However, the geometry does not affect the model parameters themselves. Therefore, the developed algorithm should yield the same identified parameters, whatever the considered geometry. In order to verify this, identification is performed successively on the experimental results of mass loss and relative humidity of G1 (P5-1), G2 (P5-2), G3 (P5-3) as well as on all results simultaneously (P5). Since the latter considers all experimental results, P5 is most likely more representative of the concrete drying behaviour. The input set of parameters for these identifications is P1. Tables 3 lists the different parameters identification trategies.

Table 2. Drying model parameters

	P1	P2	P3	P4	P5-1	P5-2	P5-3	P5
k_l	1.13E-21	1.25E-22	9.01E-22	1.54E-20	1.00E-19	9.57E-21	3.81E-21	4.68E-22
a_{vq}	4.00	1.96	100.00	10.00	6.76	6.51	5.87	2.42
b_{vq}	1.67	2.04	1.22	1.21	1.14	1.19	1.28	1.65
c_{vq}	$= 1-1/b_{vq}$	$= 1-1/b_{vq}$	$= 1-1/b_{vq}$	$= 1-1/b_{vq}$	$= 1-1/b_{vq}$	$= 1-1/b_{vq}$	$= 1-1/b_{vq}$	$= 1-1/b_{vq}$
a_{mu}	$= c_{vq}$	$= c_{vq}$	$= c_{vq}$	$= c_{vq}$	$= c_{vq}$	$= c_{vq}$	$= c_{vq}$	$= c_{vq}$
b_{mu}	0.50	-3.00	-3.00	-2.84	14.31	-3.57	-2.94	-1.57
a_{mq}	2.72	2.72	1.80	2.72	0.14	3.00	3.00	3.00
b_{mq}	4.20	2.72	1.70	4.20	2.21	5.00	5.00	3.72
h_{CL}	1.0E-05	3.3E-05	9.0E-06	1.0E-05	2.8E-06	5.4E-06	5.3E-06	1.4E-05

It is observed in Figure 11(a) that a lower drying radius results in a better identification of the drying model parameters. This is expected, since the same experiment duration was applied to all geometries. As a result, low relative humidity has already been reached in G3 at a time when G1 has higher water saturation. P5-1 exhibits a significant difference with the other parameter sets. We explain this by the fact that G1 exhibits the least advanced drying state, which makes it less reliable for determining the model parameters. For the test duration of this study (3 months), G3 is obviously more representative of the overall drying process than G1, due to its more advanced drying state.

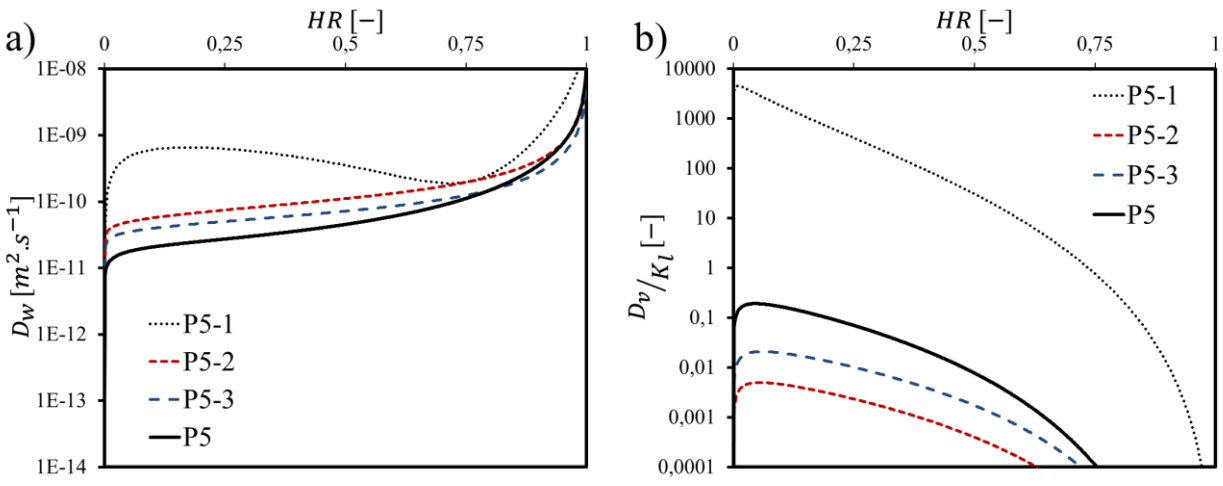

Figure 11. identification results considering only G1, G2, G3 or all of them (a) apparent coefficient of water transport as a function of relative humidity (b) diffusion to permeation ratio as a function of relative humidity

This observation is confirmed in Figure 11(b), describing the identified D_v/K_l ratio as a function of relative humidity. A D_v/K_l ratio equal to 1 indicates that water vapour diffusion and liquid water permeation are present in equal proportions. In almost all cases except P5-1, the liquid water transport mechanism is predominant, even for low relative humidity. As mentioned previously, the reason why set of parameter P5-1 deviates from this trend is due to its lower drying state.

Table 3. Different parameter identification strategies

P1	P2	P3	P4	P5	P6	P7
parameter set based from A. Hilaire [HIL14], complying with ML evolutions	manually modified parameters that comply with the ML evolution		manually modified parameters that comply both with ML and RH evolutions from G3 geometry	algorithm-identified parameters complying with ML and RH for all tested geometries	input : variable input parameters corresponding to different transport mechanisms / output : result of the identification	parameters resulting from various relative permeability, relative diffusivity and desorption isotherm models

Interestingly, the identified set of parameters P5-2 and P5-3 show a similar Dw-RH curve, indicating similar global drying physics. However, the parameters at the origin of this behaviour are quite scattered. For instance, there is a one order of magnitude difference between the intrinsic water permeability kl of P5 and P5-3 (Table 2). This is fundamental, as it still shows that although the physics are quite correctly captured by our identification tool, there are still several possible parameter sets that can yield this physical behaviour. This is why we include all 3 geometries in our reference parameter set P5.

Finally, it should be mentioned that the identified parameters P5 are within the range of values that can be found in the literature. In particular, the h_{CL} coefficient of 1.4×10^{-5} is close to the value obtained from experiments [CAR16]; the a_{mq} and b_{mq} are consistent with what is expected from cement-based materias [ZHA16]; b_{mu} is within the range suggested by [HIL14]. And more importantly, the desorption isotherm represented by parameters a_{vg}, b_{vg} and c_{vg} is close to the

experimental results for this concrete obtained by Belin *et al*. [BEL09]. This indicates that the identified solution is satisfactory both from the phenomenological and theoretical perspective. In order to fully validate the reliability of this approach, the desorption isotherm as well as relative hydraulic conductivity curves could be compared with experimental data. In order to be fully relevant, this further step should be addressed with various concrete compositions in a thorough study, and will be the object of further work.

4.2.2. *Effect of initial parameters*

In order to verify the robustness of the identification method, the effect of the input parameters on the identification output is studied. Three different cases are confronted to the reference output parameters set P5. Each one of these cases (P6-1, P6-2 and P6-3) is chosen in order to represent different water transport mechanisms. P6-1 corresponds to a large decrease of D_w, P6-2 corresponds to an increase of D_w, and P6-3 consists in lower D_w for high *RH* combined with higher D_w for low *RH*. The hydraulic conductivity resulting from these three sets of parameters are represented in Figure 12(a), showing the wide variety of transport mechanisms considered.

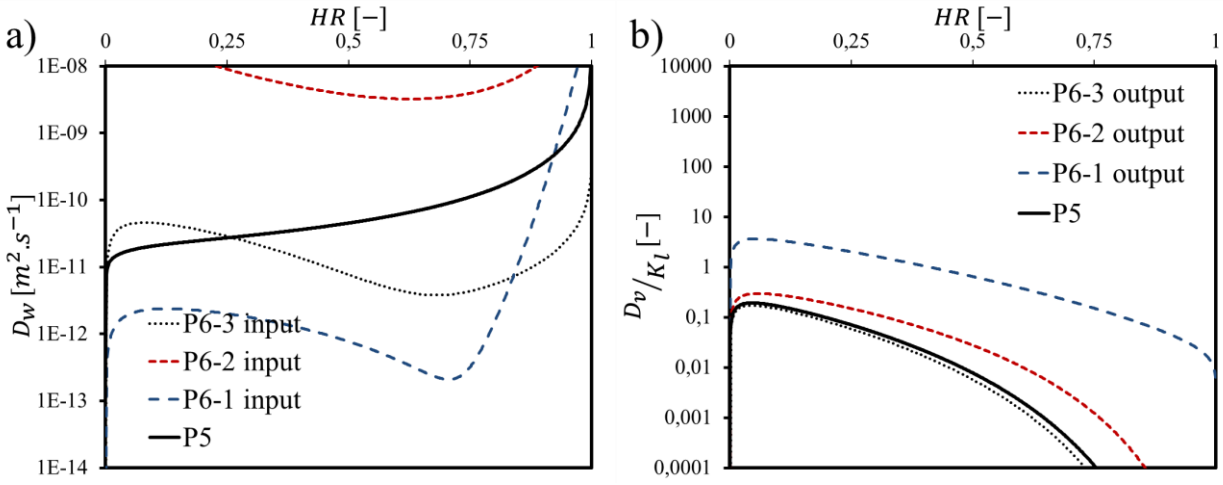

Figure 12. (a) hydraulic conductivity functions corresponding to three input sets of parameters and a reference set of parameter P5 (b) identified diffusion to permeation ratio as a function of relative humidity

The parameters corresponding to Figure 12 are displayed in Table 4. The output values are all very close to the reference case P5. The identified values of k_l, a_{vg}, b_{vg} and h_{CL} can be considered as independent from the input parameters. The main difference between the three identification scenarios is situated in the water vapour diffusion coefficient D_v. This explains the wide variations in Figure 12 (b), while the identified D_w is almost identical from P6-1, P6-2 and P6-3. The variability of D_v comes from the fact that its contribution is very low in the *RH* range corresponding to the measurements (over 45%). Therefore, the sensitivity of parameters a_{mq} and b_{mq} is very low and is therefore not reproducible in comparison with the Van Genuchten equation parameters.

Table 4. Selected input and resulting identified (output) drying model parameters

P5	P6-1 input	P6-1 output	P6-2 input	P6-2 output	P6-3 input	P6-3 output

k_l	4.68E-22	1.13E-19	4.77E-22	6.00E-21	4.69E-22	2.00E-22	4.62E-22
a_{vq}	2.42	10.00	2.41	2.00	2.42	5.00	2.41
b_{vq}	1.65	1.67	1.65	2.00	1.65	1.43	1.65
c_{vq}	*= 1-1/bvg*	*= 1-1/bvg*	*= 1-1/bvg*	*= 1-1/bvg*	*= 1-1/bvg*	*= 1-1/bvg*	*= 1-1/bvg*
a_{mu}	*= cvg*	*= cvg*	*= cvg*	*= cvg*	*= cvg*	*= cvg*	*= cvg*
b_{mu}	-1.57	10.00	-0.54	-4.00	-1.56	0.00	-1.60
a_{mq}	3.00	4.00	2.75	3.00	3.00	0.40	3.00
b_{mq}	3.72	4.20	0.16	3.00	2.42	5.00	4.05
h_{CL}	1.4E-05	1.0E-05	1.8E-05	3.3E-05	1.4E-05	1.0E-05	1.5E-05

From these results, it can be considered that according to the used drying model, and considering the mass loss and relative humidity measurements, the best fitting parameters (P5) are mostly independent on the input parameters. This unicity of solution confirms the relevance of the applied methodology.

4.2.3. *Effect of relative permeability, relative diffusivity and desorption isotherm model*

In order to study the relevance of the developed identification methodology, a last step consists in comparing different models for the relative permeability, relative diffusivity, and desorption isotherm.

Regarding the relative permeability model, four different approaches are considered. The first option consists in applying the default model, as described previously in equation (11). This model (relative permeability model 1) consists in 2 parameters to identify. The second option consists in using the same equation, but with one parameter less to identify, considering the approximation that a_{mu} is considered equal to parameter c_{vg} (relative permeability model 2). A third model is used, based on the work of Chung and Consolazio [CHU05], wherein a single parameter (a_{ch}) connects the relative permeability to the degree of saturation equation (19-20) (relative permeability model 3). Finally, a fourth possibility, also suggested by Chung and Consolazio, is particularly interesting because it involves no additional parameter to the model. It consists in fixing the value of a_{ch} as a function of the porosity of the material according to equation (21) (relative permeability model 4).

Three relative diffusivity models are considered. The first one is the default model (relative diffusivity model 1). The second one is based on the same principle (equation (13)), except that only one parameter is used instead of two, with the assumption that $b_{mq} = a_{mq} + 2$, as recommended by the authors of that model (relative diffusivity model 2) [MIL61]. Finally, the third model, shown in equation (19), is used whenever combined with relative permeability models 3 or 4, as recommenced by Chung and Consolazio (relative diffusivity model 3). This last model has the advantage of not adding parameters to the identification.

$$d_{rl}(S) = 10^{S.a_{ch}} - S.10^{a_{ch}} \tag{199}$$

$$k_{rl}(S) = d_{rl}(1 - S) \tag{20}$$

$$a_{ch} = 0.05 - 22.5\Phi \tag{21}$$

Ultimately, the desorption isotherm model is either used by default (desorption isotherm model 1) or by applying the assumption specified in equation (8). This simplification decreases the amount of parameters to identify (desorption isotherm 2).

The result of this multi-model identification is presented in Figure 13. Due to the large amount of combination of models, only the resulting hydraulic conductivity and saturation degree functions are presented, without the corresponding identified parameters. The nomenclature is as follows: $P7-ijk$ corresponds to the relative permeability model i, combined with relative diffusivity model j, and desorption isotherm model k.

As previously specified, the measured values of relative humidity do not go under 45% RH, which corresponds to the ambient relative humidity. Therefore, the identification of parameters is only relevant for RH values between 45% and 100%. This is why in Figure 13, lower RH values are shaded in gray, indicating that these values are actually not validated by our experiments.

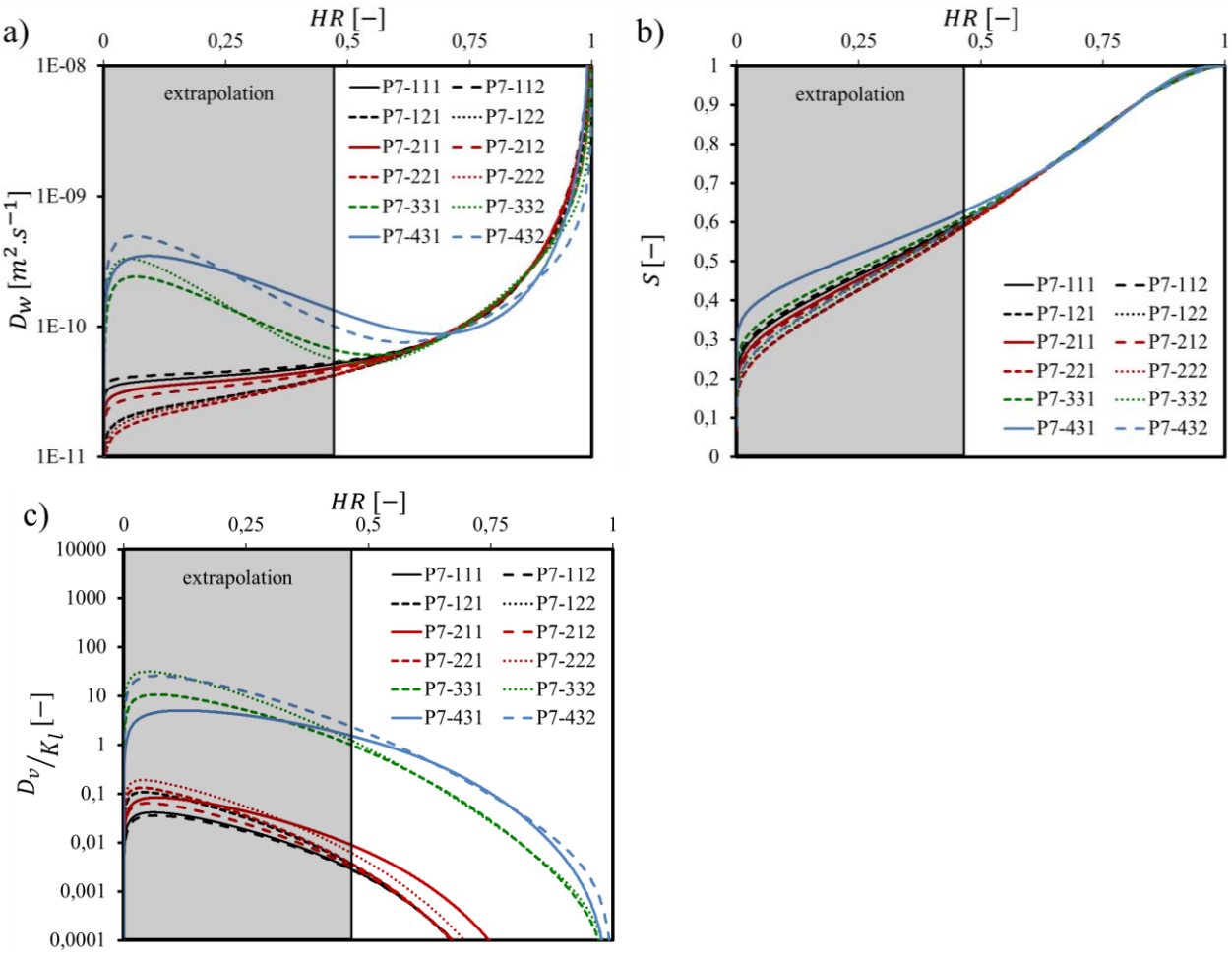

Figure 13. (a) hydraulic conductivity functions corresponding to the identified parameters from various model combinations (b) saturation degree prediction for various model combinations (c) identified diffusion to permeation ratio as a function of relative humidity

Figure 13 shows that whatever the model used among the various ones presented, the identified parameters correspond to a unique $D_w(RH)$ and $S(HR)$ relationship. At least, this is verified within the RH range that was measured experimentally. First, this indicates that the various models are versatile enough to represent the same physical reality. However, the relative contributions of vapour and liquid water transport to the hydraulic conductivity shown in Fig 13 (c) are largely affected by the relative permeability model. Indeed, models 3 and 4 (Chung and

Consolazio [CHU05]) induce a large increase in the contribution of the vapour diffusion to the hydraulic conductivity. On the other hand, the relative permeability and relative diffusivity models do not affect these respective contributions. This observation is of major importance as it shows that our current approach still requires more experimental data in order to be fully robust, especially in terms of the specific underlying mechanisms of drying in concrete.

There is therefore no preferential model among the ones who were tested, nor an optimal combination of these models. Without further validation, no model can be preferred on the basis of its predictive ability. Therefore, it seems that the model containing the least amount of parameters to identify could be preferred. Secondly, this further supports that the identification strategy that was developed in this study is robust, and yields satisfactory solutions corresponding to a global minimum of the weighed error function. The developed methodology therefore allows identifying robust and meaningful material parameters of concrete used for drying predictions.

5. Conclusion

An identification procedure for material parameters of a concrete drying model is proposed. It consists in performing a simultaneous measurement of mass loss due to the drying process as well as localised successive measurements of the relative humidity. This experimental setup is coupled with a developed identification tool able to handle several identification parameters with a specific weighed error function, combining both type of experiments. The numerical model is based on a non-linear diffusion-type model including two phenomena: liquid water permeation and water vapour diffusion. This coupled experimental and numerical approach allows identifying robust and meaningful material parameters of concrete used for drying predictions by inverse analysis.

The following conclusions are drawn:

- As expected, the mass loss measurement is not sufficient to identify the drying model parameters, since there is no unicity of solutions in regard of the amount of parameters to identify. This highly supports the necessity to include relative humidity measurements in the identification process.
- If both experimental indicators are used in the identification, the resulting material parameters are similar, whatever the experimental specimen geometry is used. Therefore, when aiming at quantifying the drying process of a new type of cement-based material, the experimental specimen geometry (and environment) should be chosen in order to accelerate as much as possible the drying process.
- If both experimental indicators are used in the identification, the resulting material parameters are independent on the input parameters. In regard of the large amount of parameters used in the identification, this shows that the solution is robust, and does not correspond to a local optimum.
- Several models are used and combined for the prediction of relative permeability and diffusivity, as well as for desorption isotherm curves. Whatever the tested combination, it is shown that the shape of the identified hydraulic conductivity and desorption isotherm is equivalent. There is therefore no preferential model among the ones which were tested.

- The relative contribution of vapour and liquid water transport is strongly dependent on the chosen relative permeability model.

Further works are required to confirm the relevance of this model for longer term experiments, as well as additional results regarding the relative humidity gradient inside the samples. This will allow a complete description of these phenomena, also an improved strategy for identifying the parameters of the model. Besides, effects of modelling choice and different relative humidity profiles, leading to the same weight loss prediction, on drying shrinkage cracking and apparent gas permeability are currently studied. This type of study could be also undertaken on the prediction of apparent diffusivity and swelling reaction (ASR, DEF for instance), which are very dependent on water content.

Acknowledgments

The authors would like to thank the IRSN for the financial support.

References

[AKI97] H. Akita, T. Fujiwara, Y. Ozaka, A practical procedure for the analysis of moisture transfer within concrete due to drying, Magazine of Concrete Research, Volume 49 (179), 129-137, 1997.

[BAO14] B.D. Liu, W. J. Lv, L. Li, P.F. Li, Effect of moisture content on static compressive elasticity modulus of concrete, Construction and Building Materials, Volume 69, 133-142, 2014

[BAR07a] V. Baroghel-Bouny, Water vapour sorption experiments on hardened cementitious materials: Part I: Essential tool for analysis of hygral behaviour and its relation to pore structure, Cement and Concrete Research, 37, 414 – 437, 2007

[BAR07b] V. Baroghel-Bouny, Water vapour sorption experiments on hardened cementitious materials. Part II: Essential tool for assessment of transport properties and for durability prediction, Cement and Concrete Research, 37, Pages 438-454, 2007

[BAZ94] Z.P. Bažant, Yunping, X., Drying creep of concrete: constitutive model and new experiments separating its mechanisms, Materials and Structures, 27, 3, 1994

[BEL09] Belin P., Bouteloup, J.-F. and Thiery, M., Caractérisation expérimentale

de diverses propriétés thermo-physico-mécaniques du béton ordinaire B11 de

Civaux. Rapport technique, Laboratoire Central des Ponts et Chaussées, 2009.

[BIS02] J Bisschop, JGM van Mier, Effect of aggregates on drying shrinkage microcracking in cement-based composites, Materials and Structures, Volume 35, 453-461, 2002

[BRI11] M. Briffaut, F. Benboudjema, J.-M. Torrenti, G. Nahas, Numerical analysis of the thermal active restrained shrinkage ring test to study the early age behavior of massive concrete structures, Engineering Structures, 33 (4), 2011, p. 1390-1401

[CAR16] Carette, J., Benboudjema F., Nahas G., Abahri K., Darquennes A., Bennacer R., Analysis of drying in concrete: effects of boundary conditions and specimen size/shape, International RILEM Conference MSSCE 2016, Copenhaguen, 2016.

[CAS07] Cast3M. Description of the finite element code Cast3M. <http://www-cast3m.cea.fr>; 2007

[CHU05] Chung, J. H., Consolazio, G. R., Numerical modelling of transport phenomena in reinforced concrete exposed to elevated temperatures. Cement and Concrete Research, 35(3):597–608, 2005

[GAM78] BR. Gamble and LJ. Parrott, Creep of concrete in compression during drying and wetting, Magazine of Concrete Research, Volume 30, N°104, Pages 129-138, 1978

[GRA14] J. Granja, M. Azenha, C. de Sousa, R. Faria, J. Barros, Hygrometric Assessment of Internal Relative Humidity in Concrete: Practical Application Issues, Journal of Advanced Concrete Technology, 12, 250-265, 2014

[HAL00] C. Hall, W. D. Hoff, Water Transport in Brick, Stone and Concrete, 2nd Edition, CRC Press, Published October 31, 2011, Reference - 374 Pages, ISBN 9780415564670-CAT# Y105780

[HIL14] Hilaire A., Etude des déformations différées des bétons en compression et en traction, du jeune au long terme : application aux enceintes de confinement, PhD Thesis, ENS Cachan, 2014

[HUA15] Q. Huang, Z.Jiang; X. Gu, W. Zhang, B. Guo, Numerical simulation of moisture transport in concrete based on a pore size distribution model, Cement and Concrete Research, 67, 31 – 43, 2015

[JER15] I. Jerjen, L. Poulikakos, M. Plamondon, P. Schuetz, T. Luethi, A. Flisch, Drying of Porous Asphalt Concrete Investigated by X-Ray Computed Tomography, Physics Procedia ,69, 451 – 456, 2015

[KIM98] J.-K. Kim, C.-S. Lee, Prediction of differential drying shrinkage in concrete, Cement and Concrete Research, Volume 28, Issue 7, Pages 985-994, 1998

[LEE08] C. Leech, D. Lockington, R.D. Hooton, G. Galloway, G. Cowin, P. Dux, Validation of mualemâs conductivity model and prediction of saturated permeability from sorptivity, ACI Materials Journal, 105(1), 2008

[MAI01] M. Mainguy, O. Coussy, V. Baroghel-Bouny, Role of air pressure in drying of weakly permeable materials, Journal of Engineering Mechanics, 127(6), 582 – 592, 2001

[MIL61] R. Millington, J. Quirk, Permeability of porous solids. Transactions of the Faraday Society, 57:1200–1207, 1961

[MON04] J. Monlouis-Bonnaire, J. Verdier, B. Perrin, Prediction of the relative permeability to gas flow of cement-based materials, Cement and Concrete Research, 34(5):737–744, 2004

[MUA76] Y. Mualem, A new model for predicting the hydraulic conductivity of unsaturated porous media. Water resources research, 12(3):513–522, 1976

[NEG15] J. Neggers, J.P.M. Hoefnagels, M. G. D. Geers, F. Hild & S. Roux. Time-resolved integrated digital image correlation. International Journal for Numerical Methods in Engineering, 2015, 103(3), 157-182.

[OXF16] M. Oxfall, P. Johansson, M. Hassanzadeh, Long-term hygrothermal performance of nuclear reactor concrete containments – Laboratory evaluations of measurement setup, in situ sampling, and moisture flux calculations, Cement and Concrete Composites , 65, 128 – 138, 2016

[OZB16] Ožbolt, J.; Oršanić, F. & Balabanić, G. Modeling influence of hysteretic moisture behavior on distribution of chlorides in concrete, Cement and Concrete Composites , 2016, 67, 73 – 84

[POP89] **S.** Popovics, Effect of Curing Method and Final Moisture Condition on Compressive Strength of Concrete. ACI Materials Journal, 83(4), 650-657, 1986

[POP05] S. Popovics, Effects of uneven moisture distribution on the strength of and wave velocity in concrete, Ultrasonics, 43, 429 – 434, 2005

[POY11] S. Poyet, S. Charles, N. Honoré V. l'Hostis, Assessment of the unsaturated water transport properties of an old concrete : Determination of the pore-interaction factor, Cement and Concrete Research, 41(10):1015–1023, 2011

[SAK83] Sakata, K. A study on moisture diffusion in drying and drying shrinkage of concrete, Cement and Concrete Research , 1983, 13, 216 – 224

[SBA07] Z. Sbartaï, S. Laurens, J. Rhazi, J. Balayssac, G. Arliguie, Using radar direct wave for concrete condition assessment: Correlation with electrical resistivity, Journal of Applied Geophysics, 62, 361 – 374, 2007

[SBA12] Z. Sbartaï, D. Breysse, M. Larget, J. Balayssac, Combining NDT techniques for improved evaluation of concrete properties, Cement and Concrete Composites, 34, 725 – 733, 2012

[THI07] M. Thiéry, V. Baroghel-Bouny, N. Bourneton, G. Villain, C. Stéfani, Modélisation du séchage des bétons - Analyse des différents modes de transfert hydrique, Revue européenne de génie civil, 11 (2007), pp. 541–577

[VAN80] M. A. van Genuchten, Closed-form Equation for Predicting the Hydraulic Conductivity of Unsaturated Soils, Soil Science Society of America Journal, 44(5):892–898, 1980

[XI94] Y. Xi, Z.P. Bažant, H. Jennings, Moisture diffusion in cementitious materials Adsorption isotherms, Advanced Cement Based Materials, 1, 248 – 257, 1994

[ZHA11] J. Zhang, D. Hou, Y. Han, Micromechanical modeling on autogenous and drying shrinkages of concrete, Construction and Building Materials, Volume 29, Pages 230-240, 2011

[ZHA15] J. Zhang, J. Wang, Y. Han, Simulation of moisture field of concrete with pre-soaked lightweight aggregate addition, Construction and Building Materials, 96, 599 – 614, 2015

[ZHA16] Z. Zhang, M. Thiery, V. Baroghel-Bouny, Investigation of moisture transport properties of cementitious materials, Cement and Concrete Research, Volume 89, Pages 257-268, 2016

[ZHA14] Z. Zhang, M. Thiéry, V. Baroghel-Bouny, A review and statistical study of existing hysteresis models for cementitious materials, Cement and Concrete Research, 57, 44 – 60, 2014

[ZHO14] C.Zhou, Predicting water permeability and relative gas permeability of unsaturated cement-based material from hydraulic diffusivity, Cement and Concrete Research, Volume 58, Pages 143-151, 2014